Detailed kinetic modeling of dimethoxymethane. Part I: *Ab initio* thermochemistry and kinetics predictions for key reactions

Wassja A. Kopp[a], Leif C. Kröger[a], Malte Döntgen[a,b], Sascha Jacobs[c], Ultan Burke[c], Henry J. Curran[d], K. Alexander Heufer[c], Kai Leonhard[a,b]

[a] *Chair of Technical Thermodynamics, RWTH Aachen University, 52062 Aachen, Germany*
[b] *AICES Graduate School, RWTH Aachen University, 52062 Aachen, Germany*
[c] *Physico-Chemical Fundamentals of Combustion, RWTH Aachen University, 52062 Aachen, Germany*
[d] *Combustion Chemistry Centre, Ryan Institute, School of Chemistry, National University of Ireland, Galway, Ireland*

Abstract

Despite the great interest in oxygenated methyl ethers as diesel fuel additives and as fuels themselves, the influence of their methylenedioxy group(s) ($O-CH_2-O$) has never been quantified using *ab initio* methods. In this study we elucidate the kinetics and thermochemistry of dimethoxymethane using high-level *ab initio* (CCSD(T)/aug-cc-pV(D+T)Z//B2PLYPD3BJ/6-311++g(d,p)) and statistical mechanics methods. We model torsional modes as hindered rotors which has a large influence on the description of the thermal behavior. Rate constants for hydrogen abstraction by $\dot{H}$ and $\dot{C}H_3$ are computed and show that abstraction from the methylenedioxy group is favored over abstraction from the terminal methyl groups. β-Scission and isomerization of the radicals is computed using master equations. The effect of rovibrationally excited radicals from preceding hydrogen abstraction reactions on subsequent hot β-scission is computed and has large influence on the decomposition of the formed dimethylether radical. In the second part of this study, the computed kinetics and thermochemistry is used in a detailed model. The quantification of the effect of the dominant methylenedioxy group using *ab initio* methods can guide modeling of oxygenated methyl ethers that contain that group several times.

Keywords: Trivialnamen: OME1, methylal; thermochemistry; hot beta scission

1. Introduction

Dimethoxymethane (DMM) is the smallest member of the family of oxygenated methyl ethers (OMEs). OMEs ($CH_3{-}O{-}(CH_2{-}O)_n{-}CH_3$) turn out to be beneficial additives for diesel fuels: They reduce soot [3, 2, 29], noise [47] and increase the efficiency by altering viscosity, lubricity, and cetane number [18]. Especially their positive influence onto the soot–NO_x tradeoff [38, 50] makes them attractive in the context of current pollutant challenges. DMM has been tested as a fuel itself [19, 22]. Its production pathways have been studied in recent years [3] and it can be produced from renewable feedstocks [40, 39], biomass [49], and CO_2 [30].

The first detailed chemical kinetic model for DMM has been obtained in 2001 by Daly *et al.* from jet-stirred reactor experiments [6]. In 2010, Dias *et al.* performed mass spectrometry studies for DMM-flames and proposed a 90-species model [8]. Experiments for high-pressure oxidation [32] and atmospheric flames [31] contribute to the recent model of Marrodán *et al.* [31]. Most hydrogen abstraction and β-scission rate constants are taken from the study of Dias *et al.* [8], which in turn have been taken from analogies from the literature. So far, no *ab initio* calculations have been conducted for the methylenedioxy group ($O{-}CH_2{-}O$) that is characteristic for OMEs.

In this work, we elucidate origin and fate of DMM radicals with *ab initio* calculations. We compute enthalpies, entropies, and heat capacities for DMM, the primary radicals ($\dot{R}1$: $\dot{C}H_2{-}O{-}CH_2{-}O{-}CH_3$ and $\dot{R}3$: $CH_3{-}O{-}\dot{C}H{-}O{-}CH_3$), $R\dot{O}_2$ and $\dot{Q}O_2H$ species. We compute rate constants for hydrogen abstraction by $\dot{H}$ and $\dot{C}H_3$ because oxidation and pyrolysis is found to be sensitive to these reactions in recent flow reactor measurements [31]. The hydrogen abstraction products are initially rovibrationally excited. If subsequent reactions as e.g. *beta*-scission take place before collisions thermalize these excited molecules, the corresponding reaction rates do not correspond to the reactants' Boltzmann distribution. We therefore not only compute thermal isomerization and β-scission but compute branching ratios for the so called hot β-scission of rovibrationally excited radicals. Altogether, these insights help to quantify the impact of the $O{-}CH_2{-}O$ group onto the combustion kinetics

of OMEs.

2. Methods

All electronic structure calculations in this study have been performed with the Gaussian09 software, revision d01 [13]. Geometries and vibrational harmonic frequencies have been obtained at the B2PLYPD3BJ/6-311++g(d,p) level for the following reasons: First, harmonic frequencies from B2PLYP have proven to outperform the widely used B3LYP frequencies [1] (used e.g. in the CBS-QB3 and the G4 compund methods). The mean unsigned error (MUE) in wavenumbers for B3LYP/N07D[1] on the F38 benchmark set amounts to $34\,\mathrm{cm}^{-1}$ [52] and for B2PLYP/N07D to $23\,\mathrm{cm}^{-1}$ [1]. Second, in addition to the fact that one should use the same method for the geometries that one uses for the frequencies, bond lengths from B2PLYP show a MUE of 0.3 Å while the MUE for B3LYP is twice as large [34]. Third, the addition of the empirical 3-parameter dispersion with Becke-Johnson damping (D3BJ) has been shown to improve reaction energies [16] and is therefore included in our density functional theory (DFT) calculations.

We compute single-point CCSD(T) energies for the geometries from the aforementioned B2PLYPD3BJ/6-311g++(d,p) level using an extrapolation of coupled-cluster energies according to:

$$E_X = \frac{a}{X^3} + E_{\mathrm{CBS}} \tag{1}$$

We use the basis sets aug-cc-pVDZ with $X = 2$ and aug-cc-pVTZ with $X = 3$ to obtain both parameters of eq. 1. This scheme yields a MUE of 0.57 kcal/mol on the DBH24/08 database of reaction barrier heights [53]. The single-reference approach is adequate for our systems because the T1-diagnostics [27] yields maximum values of 0.023 that is well below the threshold of 0.04.

We compute partition functions Q for the isobaric-isothermal ensemble (N, p, T) using the python package TAMkin [15] to derive thermal energies and entropies. In addition to

[1] The N07D basis set is constructed from addition of a reduced number of diffuse and polarization functions to the 6-31g set and is thus most comparable to the 6-311g++(d,p) basis set [17] used in this study.

the rigid rotor harmonic oscillator (RRHO) model for the stiffer stretching and bending modes, we use a one-dimensional hindered rotor model for all torsional modes. The potential energy profiles are obtained from the method used for the geometries (B2PLYPD3BJ/6-311g++(d,p)). When a lower minimum is found during the dihedral angle scan, all scans for that molecule are restarted from that lowest-energy structure. Fourier series are fitted to represent the computed potential energies as function of the corresponding dihedral angle. The number of Fourier functions is varied to yield a good compromise between deviation from the computed points and unphysical oscillations in the fitting function. The resulting potential energy function is used in a one-dimensional Schroedinger equation to compute the eigenenergies of the torsional mode. The corresponding partition function is obtained from accurate eigenvalue summation. The potential energy scans, the fitted Fourier function and the lowest energy eigenvalues for all torsional modes are depicted in the Supporting Information. We use 1000 and 2000 eigenfunctions to check whether the partition function changes at high temperature when higher energy levels are included. The increase of the number of energy levels hardly has an effect even at 4000 K. Since the hindered rotor partition function has been determined for an internal coordinate, not for a normal coordinate, the frequency that needs to be replaced is computed from the curvature at the minimum of the scan following the recommendation of Ghysels *et al.* [15].

Several torsional modes can influence each other (coupling), rendering the validity of the superposition of one-dimensional hindered rotor models questionable. Coupling will have a large effect when oxygen atoms are involved that may form intramolecular hydrogen bonds during the rotation [25]. Treating coupled degrees of freedom can be very tedious; complete coupled treatments are currently limited to seven-atomic systems [42]. Approximations still require the determination of all possible conformations. In the case of *n*-butanol this leads to 262 transition state conformations for a single abstraction channel [41]. The superposition of one-dimensional hindered rotors is shown to yield for larger alkanes errors below 1% in the entropy [46, 44]. For dimers and tetramers of alcohols, where hydrogen bonds play a key role, the superposition of one-dimensional hindered rotation yields excellent reproduction of experimental enthalpies and entropies [43]. In this study we therefore use the superposition

of one-dimensional hindered rotors as feasible means to include a large part of torsional anharmonicity.

Thermochemical values are calculated from the isobaric-isothermal (N, p, T) partition functions Q and the well-known statistical thermodynamic relations $H = RT^2 \partial \ln(Q)/\partial T$, $C_p = \partial H/\partial T$ and $S = -R \ln(Q) - H/T$ using again the TAMkin python package [15]. DeTar [7] investigated the accuracy of heat capacity and entropy obtained from *ab initio* calculations for several alkanes and found that the deviations to experimental data are mostly less than $0.5\,\mathrm{cal/(mol\,K)}$ for heat capacities and less than $0.6\,\mathrm{cal/(mol\,K)}$ for entropies.

Reaction rate constants for hydrogen abstraction are calculated using conventional transition state theory (cTST). Since the potential energy barriers and the imaginary frequencies are rather high, we expect the change of potential energy along the reaction coordinate to dominate the free energy curve and therefore variational effects to be small. Tunneling is taken into account *via* the zero-curvature Eckart approach. Eckart tunneling was shown to outperform both Wigner and Skodje & Truhlar tunneling methods [45]. Therefore we decided to use this combination of cTST / Eckart-Tunneling. Extended Arrhenius forms $k(T) = AT^n \exp(-E/T)$ are fitted[2] to reproduce the computed rate constants from 500 K to 2000 K.

Temperature- and pressure-dependent rate constants for the unimolecular isomerization and β-scission of the two DMM radicals and the dimethylether (DME) radical[3] are calculated from master equations (MEs) using the MESS software [14]. The microcanonical rate constants are calculated from Rice-Ramsperger Kassel Marcus (RRKM) theory including Eckart tunneling. Collisional energy transfer is modeled using the weak collider bath gas argon according to $\langle \Delta E_{\mathrm{down}} \rangle = 200\,\mathrm{cm^{-1}}\,(T/300\,\mathrm{K})^{0.85}$. The Lennard-Jones collision frequency [4] is calculated from $\sigma = 3.41\,\text{Å}, 5.85\,\text{Å}$, and $4.94\,\text{Å}$ and $\varepsilon = 81.1\,\mathrm{K}, 327\,\mathrm{K}$, and $275\,\mathrm{K}$ for argon, DMM, and the DME radical, respectively. All Lennard-Jones collision parameters are taken from Hippler *et al.* [21], but for DMM and the DME radical the parameters

[2]We actually fit $\ln k$ which is linear in the three parameters $\ln A$, n, and E and weights the rate constant at high temperature similarly to the rate constant at low temperature.

[3]Here, the QCISD(T)/6-31+G(d,p) information from Li *et al.* [28] was used.

for C_5H_{12} and C_3H_8 are used as close analogs, respectively. The three parameters of the modified Arrhenius form are fitted to the calculated $k(T, p)$ at various pressures from 0.01 to 100 atm.

Döntgen *et al.* [9] recently proposed the concept of hot β-scission, which describes the dissociation of rovibrationally excited fuel radicals $\dot{R}^*$ formed *via* hydrogen abstraction. Due to the excess energy available from hydrogen abstraction, the rovibrationally excited fuel radicals can dissociate faster than one would expect under the assumption of thermal equilibrium. Here, this concept is used to quantify the fraction of DMM radicals undergoing hot β-scission, using the hydrogen abstraction information generated for abstraction by $\dot{H}$ or $\dot{C}H_3$. As described by Döntgen *et al.* [9], the hydrogen abstraction rate constants can be used to compute the non-Boltzmann energy-distribution of the DMM fuel radicals, which in turn is used to weight the energy- and pressure-dependent branching ratios for β-scission obtained from the RRKM/ME simulations. These non-Boltzmann-weighted energy- and pressure-dependent branching ratios must be integrated over energy to obtain the temperature- and pressure-dependent branching ratios for hot β-scission.

3. Results and Discussion

3.1. Potential energy surface

The potential energy surface (PES) in figure 1 represents zero-point energy (ZPE)-corrected and extrapolated coupled-cluster energies as described in the methods section.

Hydrogen abstraction from the DMM molecule forms one of two radicals: Either $\dot{R}1$ ($\dot{C}H_2{-}O{-}CH_2{-}O{-}CH_3$) by abstraction from one of the two terminal CH_3 groups of DMM or $\dot{R}3$ ($CH_3{-}O{-}\dot{C}H{-}O{-}CH_3$) by abstraction from the central carbon in the methylenedioxy group. Abstraction from the methyl groups leads to the left part of the PES in figure 1; abstraction from the central carbon leads to the right part. The barrier heights for hydrogen abstraction by $\dot{H}$ are lower than the corresponding barrier heights for abstraction by $\dot{C}H_3$; for both channels the difference amounts to approximately 4 kcal/mol. The $\dot{R}3$-channel barrier is about 1 kcal/mol lower for both abstracting radicals than the barrier to the $\dot{R}1$-channel.

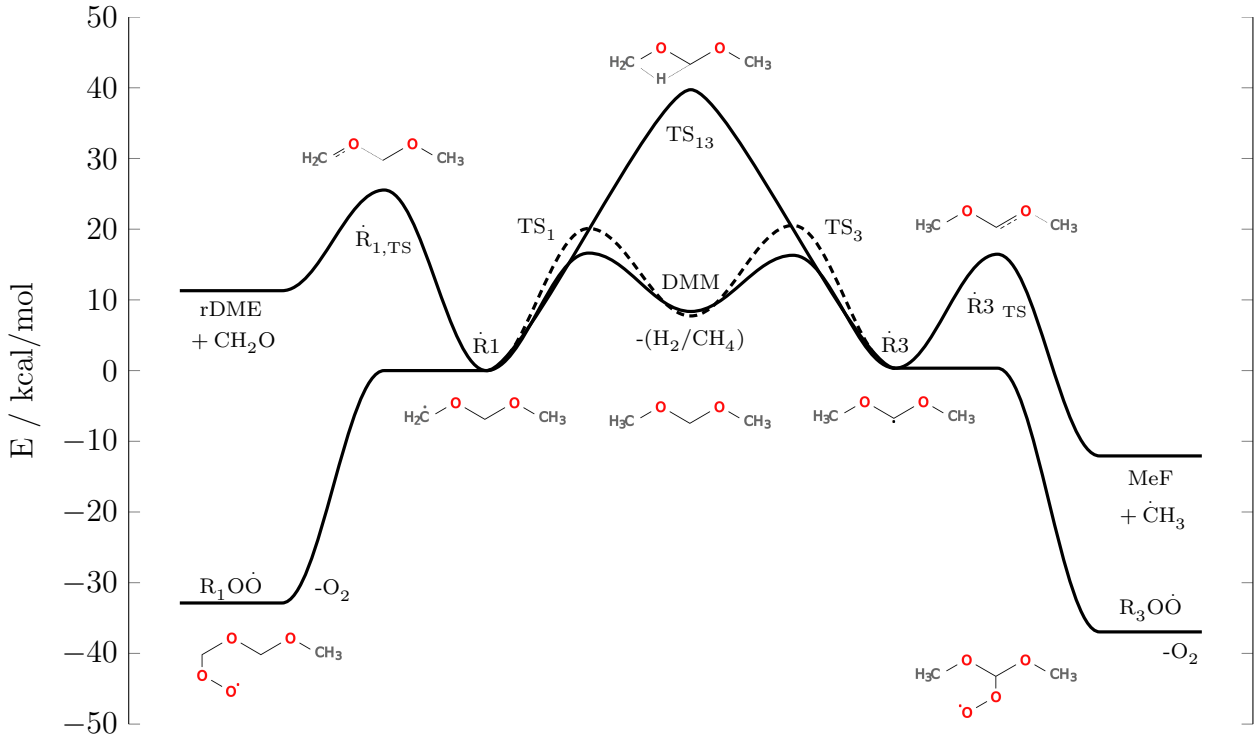

Figure 1: Potential energy surface of DMM hydrogen abstraction, radical isomerization and β-scission, and ROȮ chemistry. The zero-point of energy is located at the terminal DMM radical $\dot{\text{R}}1$; the central radical $\dot{\text{R}}3$ is 0.12 kcal/mol higher in energy. Energetic differences between systems containing different atoms are compared by subtracting the energies of the hydrogen abstraction products (H_2/CH_4) or molecular oxygen (O_2). The hydrogen abstraction transition states TS_1 and TS_3 (solid line) lie roughly 4 kcal/mol lower for abstraction by $\dot{\text{H}}$ compared to abstraction by $\dot{\text{C}}H_3$ (dashed line).

Nevertheless, abstraction from the terminal group (yielding $\dot{\text{R}}1$) offers six abstraction sites in contrast to the central carbon (yielding $\dot{\text{R}}3$), which offers only two abstraction sites. $\dot{\text{R}}1$ and $\dot{\text{R}}3$ are separated by a large barrier for isomerization. Once formed, the respective radical will therefore not isomerize but rather undergo β-scission or O_2 addition. The preferred $\dot{\text{R}}3$-pathway possesses the lower β-scission barrier of the two radicals. In fact, the barrier is of similar height as the reverse barrier for hydrogen abstraction by $\dot{\text{H}}$. This may even allow for sufficient rovibrational excitation of the $\dot{\text{R}}3$ to dissociate directly according to the concept of hot β-scission [9, 10]. We therefore expect the β-scission to be more important than the O_2 addition especially at high temperatures or under fuel-rich conditions. A quantitative

statement on the competition between DMM radical dissociation and O_2 addition, however, would require numerical simulations that are planned for the second part of this study [23].

3.2. Thermochemistry

We calculated enthalpies, entropies, and heat capacities as described in the methods section for use in detailed combustion models. We fitted NASA-polynomial expressions from 100 K to 1000 K and from 1000 K to 4000 K to our calculated values and report them in the supporting information. The largest deviations of the fit from the calculation amount to 0.073 kcal/mol for the enthalpies and to 0.128 cal/(mol K) for the entropies.

Despite our expectation of O_2 addition to be not prominent under various conditions, we calculated thermochemical data for the fuel (RH), fuel radicals ($\dot{R}$), fuel radical peroxides ($R\dot{O}_2$), and internal hydrogen abstraction products ($\dot{Q}O_2H$). In addition, to allow for comparison with group additivity schemes for non-radical substances, we calculated RO_2H species. Experimental values exist for a few substances, so that we can compare the respective calculated values: Pilcher and Fletcher [37] measured the DMM heat of combustion in a flame calorimeter from which one can compute the heat of formation to be −83.21 kcal/mol. Our calculated value (cf. table 1) is 1.09 kcal/mol higher. The standard entropy of DMM has been determined from calorimeter experiments by McEachern Jr. and Kilpatrick [24] to amount to 80.24 cal/(mol K). Our calculated value is 1.07 cal/(mol K) lower. For the radical $\dot{R}3$, the enthalpy of formation is 0.4 kcal/mol higher than for the terminal DMM radical $\dot{R}1$. For this central radical $\dot{R}3$, we can make a comparison to the structurally similar DME. Yamada *et al.* [48] determined thermodynamic properties for the $CH_3OCH_3 + O_2$ reaction system using isodesmic reactions, CBS-q and G2 calculations and the experimental DME data from Stull *et al* [26]. The C−H bond-dissociation energy (BDE) at the central group of DMM is 1.1 kcal/mol higher than the BDE of DME. Subsequent O_2 addition to the $\dot{R}3$ radical of DMM releases 4.13 kcal/mol more enthalpy than the analogous process for DME. Internal hydrogen abstraction from the other methyl group in DME requires an energy of 8.4 kcal/mol. The comparison to DMM (yielding 8.9 kcal/mol) does not involve the same groups: The $\dot{Q}1O_2H$ (cf. figure 2(a)) involves internal hydrogen abstraction from the central

Species Quantity	h_f(298.15 K)	s^0(298.15 K)	c_p				
			298.15 K	500 K	1000 K	1500 K	2000 K
RH	-82.125	79.170	25.50	36.52	50.78	58.75	62.58
RH [37]	-83.21	80.24	-	-	-	-	-
CH_3OCH_3 [26, 48]	-43.99	-	-	-	-	-	-
$\dot{R}1$	-37.352	81.737	26.27	35.68	47.49	53.71	56.89
$\dot{R}3$	-36.927	84.680	25.23	33.53	46.57	53.54	57.18
$CH_3O\dot{C}H_2$ [48]	0.1	67.67	14.79[4]	20.74	30.10	34.84	-
$R1\dot{O}_2$	-71.352	96.822	31.62	43.77	57.55	64.77	67.81
$R3\dot{O}_2$	-75.061	93.882	32.32	42.73	57.05	63.31	66.40
$CH_3OCH_2OO\cdot$ [48]	-33.9	83.1	21.34	29.30	40.36	45.51	-
$R1O_2H_2H$	-110.905	87.266	30.77	47.93	68.89	74.41	76.24
$R3O_2H_2H$	-111.053	94.719	35.28	46.78	62.23	69.38	72.99
CH_3OCH_2OOH [48]	-70.7	-	-	-	-	-	-
$\dot{Q}1O_2H$	-62.910	93.982	34.07	46.57	61.25	66.57	69.05
$\dot{Q}1fO_2H$	-63.616	90.571	34.52	49.87	64.48	68.45	70.04
$\dot{Q}3O_2H$	-65.330	92.865	36.02	48.20	59.75	65.39	68.17
$\dot{C}H_2OCH_2OOH$ [48]	-26.5	88.02	22.99	31.38	41.20	45.41	-

Table 1: standard heats of formation are reported in kcal / mol; entropies and heat capacities are reported in cal / (mol K).

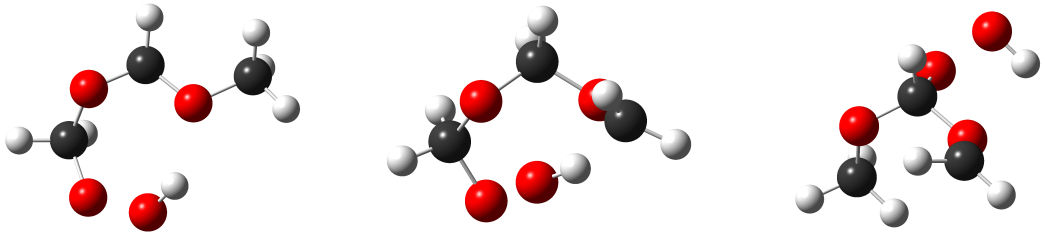

(a) $Q1O_2H$ (b) $Q1O_2H$ far side (c) $Q3O_2H$

Figure 2: Three possible products of internal hydrogen abstraction in the RO_2.

methylenedioxy group that is different from the methyl group in DME. Structurally more similar to the DME case is perhaps the internal hydrogen abstraction in $\dot{R}1$ from the "far" carbon, yielding $\dot{Q}1fO_2H$ ($\dot{C}H_2-O-CH_2-O-CH_2O_2H$, cf. figure 2(b)). The formation of QO_2Hf requires an enthalpy uptake of 7.736 kcal/mol. This substance is not formed *via* a six-membered ring transition state (TS) and therefore probably produced at lower rate. Nevertheless, its thermochemistry can be included in detailed models.

Yamada *et al.* calculated the standard enthalpy of formation for the RO_2H of DME from CBS-q calculations *via* isodesmic reactions [48]. Incorporating O_2 into the DME fuel molecule would thus release an energy of 26.7 kcal/mol. The same process in the DMM molecule would release an energy of 28.8 kcal/mol at the 1-site and of 28.9 kcal/mol at the 3-site. All in all, the computed thermochemical data agrees with available experiments and similar species mostly within 1 kcal/mol uncertainty.

3.3. H-atom abstraction

We fit three-parameter Arrhenius expressions to the rate constants calculated from cTST in steps of 100 K from 500 K to 2000 K. The maximum deviation of the fitted rate constants from the calculated ones amounts to 4%. The expressions read for the four possible abstrac-

tions (2 radicals at 2 sites):

$$\mathrm{RH} + \dot{\mathrm{H}} \longrightarrow \dot{\mathrm{R}}1 + \mathrm{H_2} \tag{2}$$

$$k_2(T) = 2.2966 \times 10^4\,\mathrm{cm^3/(mol\,s)} T^{2.8977} \exp\left(-2618.33\,\mathrm{K}/T\right)$$

$$\mathrm{RH} + \dot{\mathrm{H}} \longrightarrow \dot{\mathrm{R}}3 + \mathrm{H_2} \tag{3}$$

$$k_3(T) = 5.2069 \times 10^7\,\mathrm{cm^3/(mol\,s)} T^{1.8855} \exp\left(-2645.08\,\mathrm{K}/T\right)$$

$$\mathrm{RH} + \dot{\mathrm{C}}\mathrm{H_3} \longrightarrow \dot{\mathrm{R}}1 + \mathrm{CH_4} \tag{4}$$

$$k_4(T) = 1.4580 \times 10^{-2}\,\mathrm{cm^3/(mol\,s)} T^{4.2458} \exp\left(-3795.91\,\mathrm{K}/T\right)$$

$$\mathrm{RH} + \dot{\mathrm{C}}\mathrm{H_3} \longrightarrow \dot{\mathrm{R}}3 + \mathrm{CH_4} \tag{5}$$

$$k_5(T) = 1.3013 \times 10^2\,\mathrm{cm^3/(mol\,s)} T^{3.1234} \exp\left(-4018.26\,\mathrm{K}/T\right)$$

(6)

Tunneling increases the rate constants by factors up to 3.5 at 500 K. At higher temperatures, tunneling still plays a role for abstraction by $\dot{\mathrm{C}}\mathrm{H_3}$. At 1000 K, the rate is increased by 35%. Hindered rotation affects especially the 3-site by factors up to 3.8.

From 500 K to 2000 K (cf. figure 3) abstraction from the 3-site is always faster than from the 1-site for both abstracting radicals, as expected from the PES. Although there are 6 hydrogens to abstract from the 1-site compared to 2 hydrogens at the 3-site, the effect of the weakened C−H bond at the central carbon dominates. Rate constants for abstraction by $\dot{\mathrm{H}}$ are always larger than those for abstraction by $\dot{\mathrm{C}}\mathrm{H_3}$. We compare our rate constants to the rate constants of the mechanism by Marrodán [31] *et al.* from 2016. These in turn are the same for the reactions considered here as in the first detailed DMM model of Daly [6] *et al.* from 2001, except for $\mathrm{RH} + \dot{\mathrm{H}} \longrightarrow \dot{\mathrm{R}}3 + \mathrm{H_2}$ where the frequency parameter A was slightly decreased. We speak of rate constants calculated in this study by *ab initio* methods as of "calculated" rate constants while we speak of rate constants from the literature that stem from estimations based on analogies to similar compounds or groups, eventually altered in light of experiments, as of "modeled" rate constants. For abstraction by $\dot{\mathrm{H}}$, the calculated rate constants coincide with the modeled rate constants for the 1-site at 2000 K and for the 3-site at about 900 K. At other temperatures, the

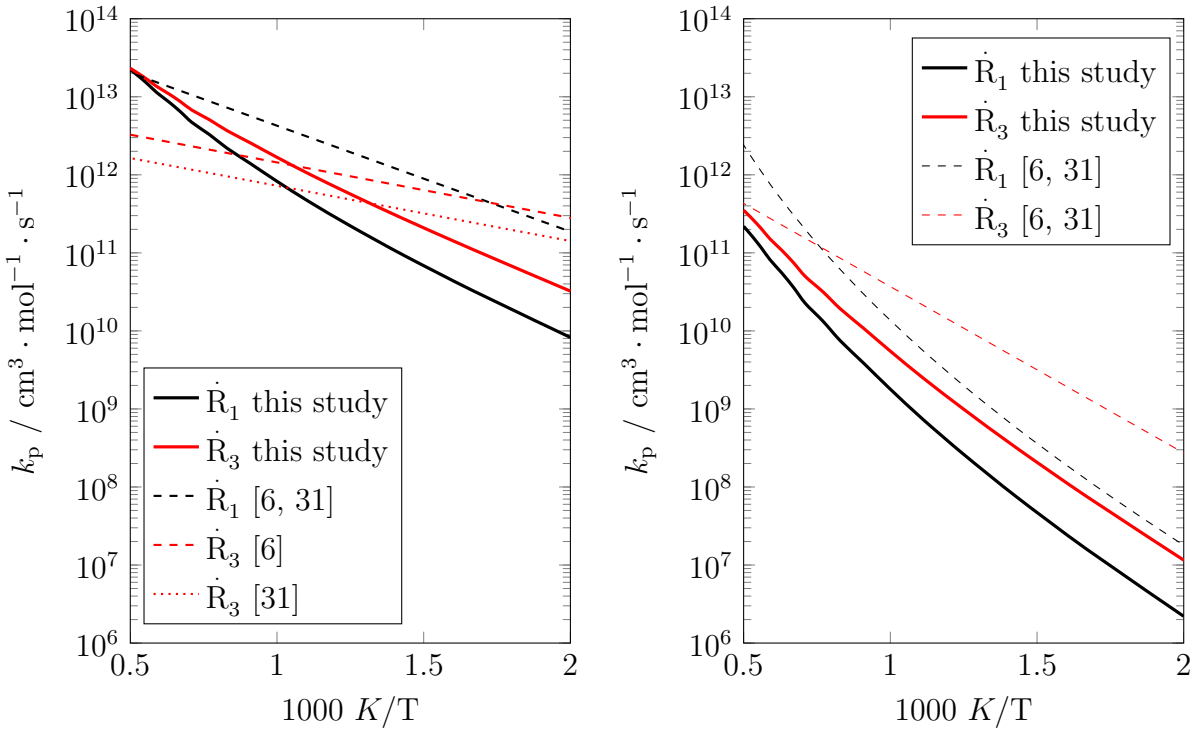

(a) $\mathrm{RH} + \dot{\mathrm{H}} \longrightarrow \dot{\mathrm{R}} + \mathrm{H_2}$

(b) $\mathrm{RH} + \dot{\mathrm{C}}\mathrm{H_3} \longrightarrow \dot{\mathrm{R}} + \mathrm{CH_4}$

Figure 3: Site-specific rate constants for hydrogen abstraction from DMM. The solid lines are the ones computed in this study, the dashed and dotted lines refer to the rate constants modeled by Marrodán *et al.* [31] and by Daly *et al.* [6].

calculated and modeled rates differ up to one order of magnitude. This affects especially the branching ratio: While our calculations show that abstraction by $\dot{\mathrm{H}}$ produces mostly $\dot{\mathrm{R}}3$, the previously modeled rates would favor $\dot{\mathrm{R}}1$. For abstraction by $\dot{\mathrm{C}}\mathrm{H_3}$, the modeled branching ratio favors $\dot{\mathrm{R}}1$ above approximately 1200 K. For this abstraction, the modeled rate constants are approximately one order of magnitude larger than our calculated ones. In conclusion, the calculated hydrogen abstraction rates are mostly slower than previous estimations and always favor abstraction from the methylenedioxy group. This can have large consequences on the resulting species pool because of the different subsequent β-scission products of the two radicals. We expect an increased formation of C=O containing species instead of ether radicals. A similar finding was observed in reactive molecular dynamics simulations of larger OMEs [11]. Larger OMEs contain the methylenedioxy group several times so that the

consequences that we discuss for the branching ratio can be even more severe.

3.4. Unimolecular radical kinetics

The ME calculations confirm our earlier assumption based on the PES data that both radicals do not isomerize but rather undergo β-scission. Isomerization is computed to be fastest at high pressure. The Arrhenius equation for the isomerization of $\dot{\text{R}}1$ to $\dot{\text{R}}3$ at 100 atm is given by $k(T) = 2.9 \times 10^{-29}/\text{s} T^{11.8} \exp\left(-11\,823\,\text{K}/T\right)$ which reproduces the rate between 500 K and 1000 K. The reverse rate, i.e. isomerization of $\dot{\text{R}}3$ to $\dot{\text{R}}1$ is always slightly slower. This is consistent with the higher standard entropy of $\dot{\text{R}}3$ and underlines again the key role of the central radical $\dot{\text{R}}3$. The isomerization rate constants in that temperature and pressure region remain below $1\,\text{cm}^3/(\text{mol}\,\text{s})$, that is more than six orders of magnitude below the β-scission rate for $\dot{\text{R}}3$. We therefore do not discuss the isomerization of the DMM radicals any further.

The β-scission rate constants for both radicals show strong temperature- and pressure-dependent fall-off. The fall-off for $\dot{\text{R}}3$ is shown in figure 4; the behavior of $\dot{\text{R}}1$ is not depicted since it is very similar and that radical is not prominent compared to $\dot{\text{R}}3$. As expected, the fall-off is getting stronger with increasing temperature and decreasing pressure. Even at very high pressures of 100 atm, the β-scission rate of $\dot{\text{R}}3$ at 700 K is a factor of 2 below the high-pressure limit and at 1000 K a factor of four below the high-pressure limit.

We can compare the rate constants as function of temperature and pressure to high-pressure limits for similar substances that are available in the literature (cf. figure 5): For $\dot{\text{R}}1$, the decomposition kinetics of the DME radical reported by Li *et al.* [28] are used as a reference due to the similar terminal $-\dot{\text{C}}\text{H}_2$ group. For $\dot{\text{R}}3$, the decomposition kinetics of the diethylether (DEE) radical reported by Yasunaga *et al.* [51] are used as a reference because the $-\dot{\text{C}}\text{H}-$ group can serve as closest analog. While the high-pressure limit of $\dot{\text{R}}1$ β-scission can be reproduced reasonably well with the analogy to DME, the analogy to DEE for $\dot{\text{R}}3$ is off by a factor of two which shows once more the special behavior of the methylenedioxy group. Over large temperature ranges, the modeled rate constants resemble closer the data at pressures between 10 atm to 100 atm, staying below the calculated high-pressure limit at all

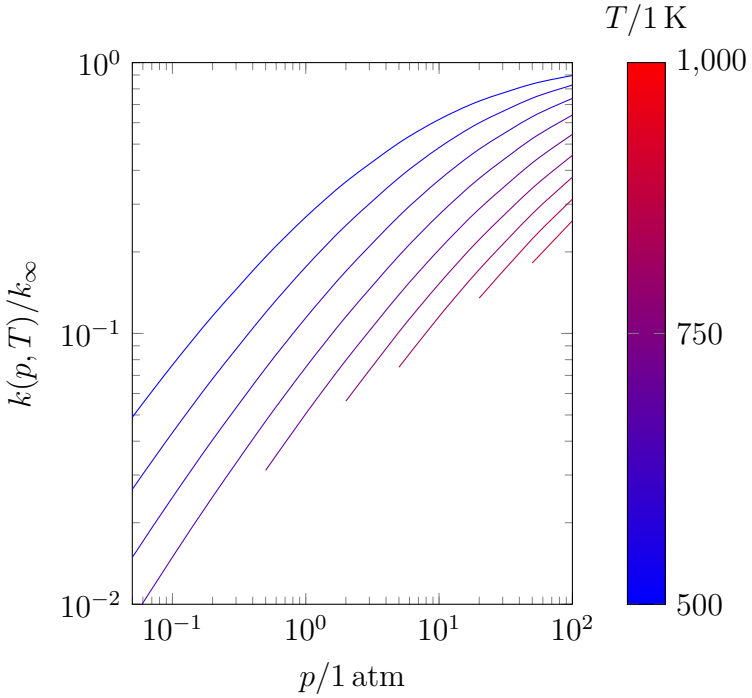

Figure 4: Isotherms of the T, p-dependent fall-off behavior of thermal β-scission rate constants of $\dot{\mathrm{R}}_3$.

investigated temperatures. Both pathways exhibit major fall-off: The rate constants partly drop by almost three orders of magnitude. To model the DMM radical kinetics accurately, it therefore appears essential to include highly resolved pressure dependence. At low pressures, the DMM radicals become chemically ill-defined with increasing temperature [10]. This is due to the inseparability of chemical and collisional eigenvalues of the master equation at low pressures and high temperatures [33]. The ends of the lines in figures 4 and 5 indicate this region.

3.5. Hot unimolecular reactions

β-Scission following a precedent exothermic hydrogen abstraction may take place faster if the rovibrationally excited radicals are not completely thermalized by collisions. This process is called hot β-scission [9]. The β-scission products in turn can undergo hot β-scission again, using the excess energy from hydrogen abstraction firstly, and from the radical dissociation secondly. The products of the two β-scission pathways in DMM are substantially

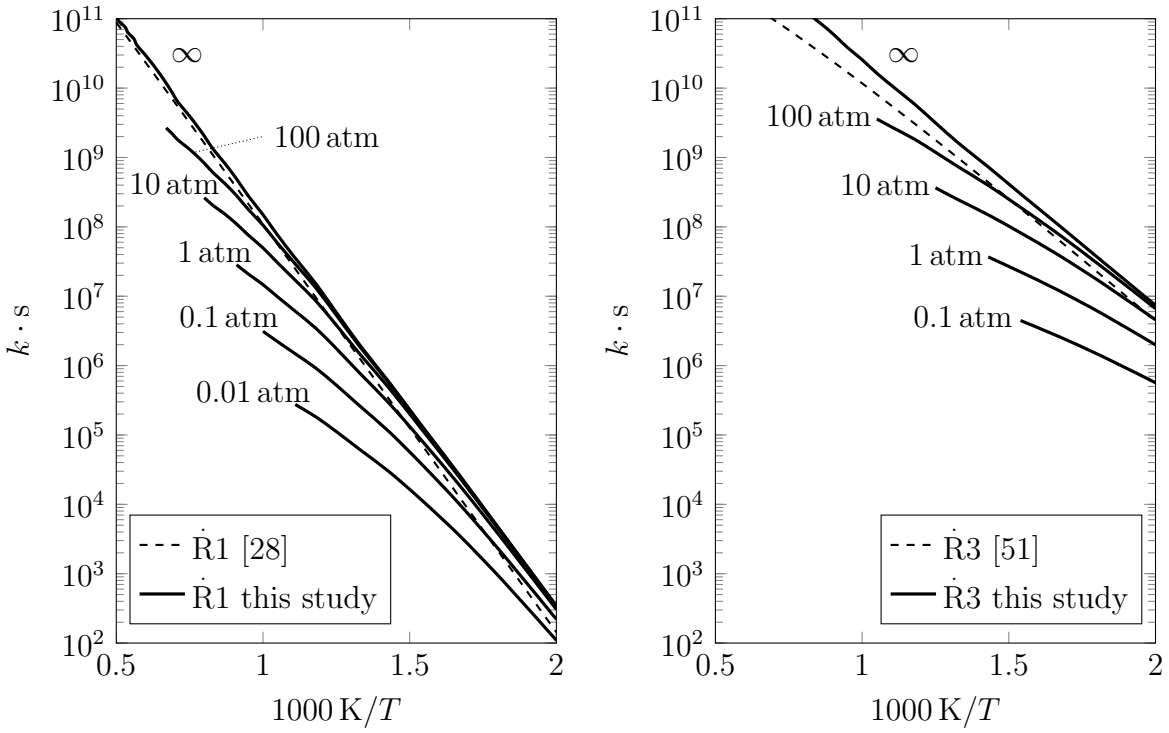

(a) $\dot{\mathrm{R}}1 \longrightarrow \mathrm{CH_2O} + \mathrm{rDME}$

(b) $\dot{\mathrm{R}}3 \longrightarrow \dot{\mathrm{C}}\mathrm{H_3} + \mathrm{MeF}$

Figure 5: Temperature- and pressure-depending rate constants for thermal β-scission of $\dot{\mathrm{R}}1$ and $\dot{\mathrm{R}}3$ (solid lines). Reference rate constants for β-scission of $\dot{\mathrm{R}}1$ and $\dot{\mathrm{R}}3$ are taken from rDME $\longrightarrow \dot{\mathrm{C}}\mathrm{H_3} + \mathrm{CH_2O}$ by Li *et al.* [28] and from rDEE $\longrightarrow \dot{\mathrm{C}}\mathrm{H_2CH_3} + \mathrm{CH_3CHO}$ by Yasunaga *et al.* [51], respectively (dashed lines).

different. The product of $\dot{\mathrm{R}}3$ β-scission, methyl format (MF), does not show negative-temperature coefficient (NTC) behavior in ignition delay time measurements [12]. Dissociation of MF is very unlikely (the smallest dissociation limit amounts to 68.05 kcal/mol [35]). In contrast, the product of $\dot{\mathrm{R}}1$ β-scission, dimethylether radical (rDME), shows rich low-temperature chemistry and a NTC regime [20, 5, 36]. It possesses a β-scission barrier of only 25.90 kcal/mol [28].

Temperature- and pressure-dependent branching ratios for hot β-scission of DMM radical $\dot{\mathrm{R}}3$ formed *via* hydrogen abstraction by $\dot{\mathrm{C}}\mathrm{H_3}$ are shown in figure 6. The branching ratio refers to the fraction of DMM that reacts to β-scission products *via* the hot route compared to the total amount of DMM that reacts *via* hydrogen abstraction by $\dot{\mathrm{C}}\mathrm{H_3}$ and both kinds

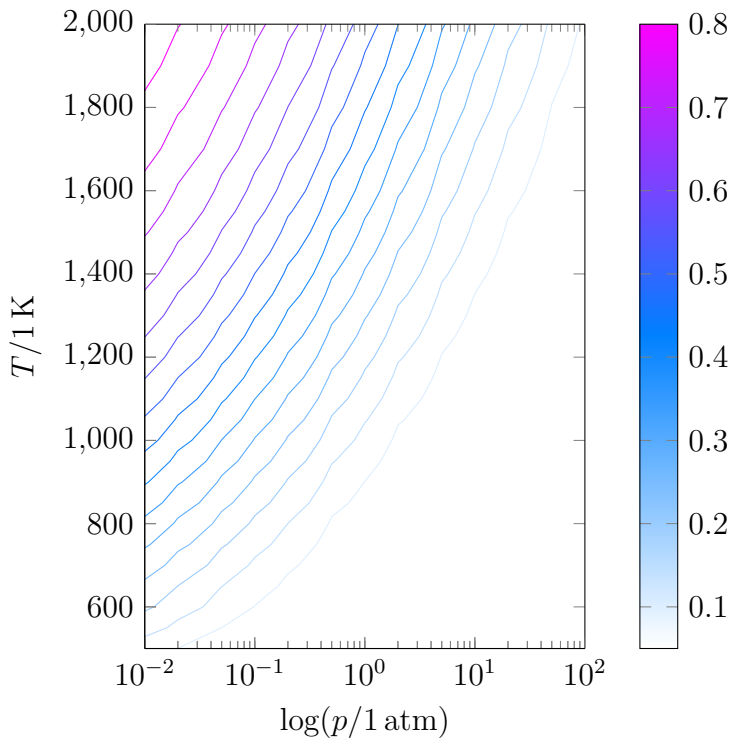

Figure 6: Temperature- and pressure-depending branching ratios for hot β-scission of the $\dot{\mathrm{R}}_3$ formed *via* hydrogen abstraction by $\dot{\mathrm{C}}\mathrm{H}_3$.

of subsequent β-scission. Some parts of the figure appear to have a step-wise nature, which results from the temperature- and pressure-discretization of the ME simulations and has no physical reasoning. Hot β-scission of $\dot{\mathrm{R}}3$ formed *via* hydrogen abstraction by $\dot{\mathrm{H}}$ is similar to that shown in Figure 6, but the branching ratios are roughly 50 % smaller. In case that chemical and relaxational eigenvalues of the ME are indistinguishable, the approximate scheme proposed by Döntgen *et al.* [10] is used to estimate the branching ratios. With this approximation, the branching ratios are obtained *via* utilization of the energy-dependent branching ratios of the highest temperature and lowest pressures for which the ME eigenvalues can be still clearly separated. In reality, the energy-dependent branching ratios would slightly change with increasing temperature, increasing the fraction of rovibrationally excited radicals going the hot route [10]. Thus, this approximation will underestimate hot β-scission branching ratios. Although hot β-scission of $\dot{\mathrm{R}}1$ can be neglected at any presently

studied condition, rDME formed *via* thermal $\dot{\text{R}}1$ β-scission is found to partly dissociate *via* hot β-scission as shown in figure 7. For the dissociation of rDME, the barrier is 12 kcal/mol

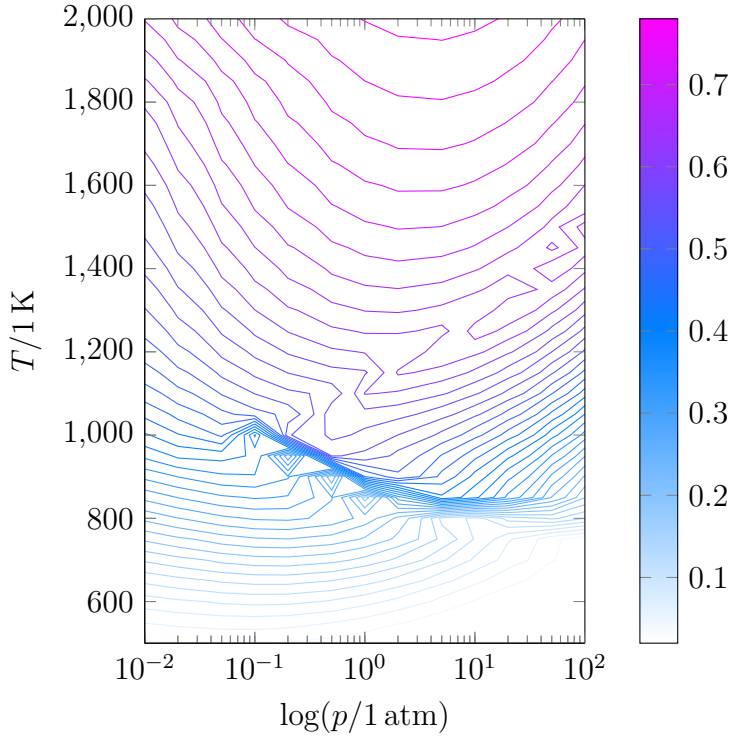

Figure 7: Temperature- and pressure-depending branching ratios for hot β-scission of the DME radical formed *via* dissociation of DMM radical $\dot{\text{R}}1$. The unsteady parts of the plot result from numerical issues of the ME simulations; we interpolated linearly where there were jumps due to numerical reasons in the ME.

higher than the β-scission barrier of $\dot{\text{R}}1$. Still, a significant amount (about 10% above 600 K) of rDME undergoes hot β-scission. With increasing temperature, the branching ratio for hot β-scission becomes larger. More than 25% of rDME dissociate *via* the hot route above 800 K (cf. figure 7). The pressure-dependence of rDME hot β-scission exhibits a minimum with respect to pressure (cf. the minima of the isolines in figure 7). These minima could potentially result from the interplay of the increasing amount of rDME radicals being formed as pressure increases and the decreasing lifetime of the rovibrationally excited rDME radicals. As a consequence, more rovibrationally excited rDME radicals are formed with increasing pressure, until thermalization becomes stronger.

In conclusion, hot β-scission can influence the $\dot{\text{R}}3$ channel in flames at high temperatures

and low pressures. The $\dot{R}1$ channel is not affected by hot β-scission at all. The resulting rDME radicals of the $\dot{R}1$ channel in turn favor hot β-scission even at engine-relevant conditions. This increased consumption of rDME will make the O_2 low-temperature chemistry path even less important in the combustion of DMM.

4. Conclusions

The central DMM radical $\dot{R}3$ is the favored product of hydrogen abstraction: While the enthalpy of formation for $\dot{R}3$ is higher than for the terminal DMM radical $\dot{R}1$, the abstraction barrier for abstraction by $\dot{H}$ and by $\dot{C}H_3$ is both 1 kcal/mol smaller for $\dot{R}3$ than for $\dot{R}1$. The branching ratios for hydrogen abstraction – in contrast to previous models – suggest that formation of $\dot{R}3$ is always favored. Subsequent β-scission of $\dot{R}3$ yields MF, which does not show NTC-behavior. The MF formation is even more favored considering hot β-scission. The rDME formed from $\dot{R}1$ is especially prone to hot β-scission, but less important since $\dot{R}1$ plays an inferior role. The unimolecular pathways show strong pressure dependence. Especially the β-scission of the dominant $\dot{R}3$ radical is far from its high-pressure limit even at 100 atm. Computed thermochemical values for DMM, its radicals, and subsequent species agree with experimental values and analogs from DME within about 1 kcal/mol uncertainty. The present insights into the kinetics and thermochemistry of DMM and its radicals will allow for more accurate mechanism development (subject to the second part of this work [23]), especially concerning low-temperature chemistry. The quantification of the impact of the methylenedioxy group on kinetics will improve modeling of larger OMEs.

Appendix A. Acknowledgements

This work was performed as part of the Cluster of Excellence "Tailor-Made Fuels from Biomass" (EXC 236), which is funded by the Excellence Initiative by the German federal and state governments to promote science and research at German universities. We gratefully acknowledge CPU time grant rwth0070 of the RWTH Aachen University Compute Cluster. MD is thankful for financial support from the Deutsche Forschungsgemeinschaft (German Research Association) through grant GSC 111.

Appendix B. References

[1] Biczysko, M., Panek, P., Scalmani, G., Bloino, J., and Barone, V. Harmonic and anharmonic vibrational frequency calculations with the double-hybrid b2plyp method: Analytic second derivatives and benchmark studies. *J. Chem. Theory Comput. 6* (2010), 2115–2125.

[2] Burger, J., and Hasse, H. Multi-objective optimization using reduced models in conceptual design of a fuel additive production process. *Chem. Eng. Sci. 99* (2013), 118 – 126.

[3] Burger, J., Siegert, M., Stroefer, E., and Hasse, H. Poly(oxymethylene) dimethyl ethers as components of tailored diesel fuel: Properties, synthesis and purification concepts. *Fuel 89*, 11 (NOV 2010), 3315–3319.

[4] Carstensen, H.-H., and Dean, A. M. The kinetics of pressure-dependent reactions. *Comprehensive Chemical Kinetics 42* (2007), 105–187.

[5] Curran, H. J., Fischer, S. L., and Dryer, F. L. The reaction kinetics of dimethyl ether. II: Low-temperature oxidation in flow reactors. *Int. J. Chem. Kinet. 32*, 12 (DEC 2000), 741–759.

[6] Daly, C. A., Simmie, J. M., Dagaut, P., and Cathonnet, M. Oxidation of dimethoxymethane in a jet-stirred reactor. *Combust. Flame 125*, 3 (2001), 1106 – 1117.

[7] DeTar, D. F. Theoretical ab initio calculation of entropy, heat capacity, and heat content. *J. Phys. Chem. A 102* (1998), 5128–5141.

[8] Dias, V., Lories, X., and Vandooren, J. Lean and rich premixed dimethoxymethane/oxygen/argon flames: Experimental and modeling. *Combust. Sci. Technol. 182*, 4-6 (2010), 350–364.

[9] Döntgen, M., Kröger, L. C., and Leonhard, K. Hot β-scission of radicals formed via hydrogen abstraction. *Proc. Combust. Inst. 36* (2017), 135–142.

[10] Döntgen, M., and Leonhard, K. Discussion of the separation of chemical and relaxational kinetics of chemically activated intermediates in master equation simulations. *J. Phys. Chem. A 121* (2017), 1563–1570.

[11] Döntgen, M., Wächter, D., and Leonhard, K. Dissociation cascades of oxymethylene ethers. *J. Chem. Phys. Lett.* (2017). to be submitted.

[12] Fisher, E. M., Pitz, W. J., Curran, H. J., and Westbrook, C. K. Detailed chemical kinetic mechanisms for combustion of oxygenated fuels. *Proc. Combust. Inst. 28* (2000), 1579 – 1586.

[13] Frisch, M. J., Trucks, G. W., Schlegel, H. B., Scuseria, G. E., Robb, M. A., Cheeseman, J. R., Scalmani, G., Barone, V., Mennucci, B., Petersson, G. A., Nakatsuji, H., Caricato, M., Li, X., Hratchian, H. P., Izmaylov, A. F., Bloino, J., Zheng, G., Sonnenberg, J. L., Hada, M., Ehara, M., Toyota, K., Fukuda, R., Hasegawa, J., Ishida, M., Nakajima, T., Honda, Y., Kitao, O., Nakai, H., Vreven, T., Montgomery, Jr., J. A., Peralta, J. E., Ogliaro, F., Bearpark, M., Heyd, J. J., Brothers, E., Kudin, K. N., Staroverov, V. N., Kobayashi, R., Normand, J., Raghavachari, K., Rendell, A., Burant, J. C., Iyengar, S. S.,

Tomasi, J., Cossi, M., Rega, N., Millam, J. M., Klene, M., Knox, J. E., Cross, J. B., Bakken, V., Adamo, C., Jaramillo, J., Gomperts, R., Stratmann, R. E., Yazyev, O., Austin, A. J., Cammi, R., Pomelli, C., Ochterski, J. W., Martin, R. L., Morokuma, K., Zakrzewski, V. G., Voth, G. A., Salvador, P., Dannenberg, J. J., Dapprich, S., Daniels, A. D., Farkas, O., Foresman, J. B., Ortiz, J. V., Cioslowski, J., and Fox, D. J. Gaussian 09 Revision A.1, 2009. Gaussian Inc. Wallingford CT 2009.

[14] Georgievskii, Y., Miller, J. A., Burke, M. P., and Klippenstein, S. J. Reformulation and solution of the master equation for multiple-well chemical reactions. *J. Phys. Chem. A 117* (2013), 12146.

[15] Ghysels, A., Verstraelen, T., Hemelsoet, K., Waroquier, M., and Van Speybroeck, V. TAMkin: A Versatile Package for Vibrational Analysis and Chemical Kinetics. *J. Chem. Inf. Model. 50* (2010), 1736–1750.

[16] Grimme, S., Ehrlich, S., and Goerigk, L. Effect of the Damping Function in Dispersion Corrected Density Functional Theory. *J. Comput. Chem. 32*, 7 (MAY 2011), 1456–1465.

[17] Hariharan, P. C., and Pople, J. A. The influence of polarization functions on molecular orbital hydrogenation energies. *Theoret. chim. Acta 28*, 3 (1973), 213–222.

[18] Härtl, M., Seidenspinner, P., Jacob, E., and Wachtmeister, G. Oxygenate screening on a heavy-duty diesel engine and emission characteristics of highly oxygenated oxymethylene ether fuel. *Fuel 153* (2015), 328 – 335.

[19] Härtl, M., Seidenspinner, P., Wachtmeister, G., and Jacob, E. Synthetischer dieselkraftstoff ome1 — lösungsansatz für den zielkonflikt nox-/partikel-emission. *MTZ - Motortechnische Zeitschrift 75*, 7 (2014), 68–73.

[20] Herrmann, F., Jochim, B., Owald, P., Cai, L., Pitsch, H., and Kohse-Hinghaus, K. Experimental and numerical low-temperature oxidation study of ethanol and dimethyl ether. *Combust. Flame 161*, 2 (2014), 384 – 397.

[21] Hippler, H., Troe, J., and Wendelken, H. J. Collisional deactivation of vibrationally highly excited polyatomic molecules. II. direct observations of excited toluene. *J. Chem. Phys. 78* (1983), 6709.

[22] Iannuzzi, S. E., Barro, C., Boulouchos, K., and Burger, J. Combustion behavior and soot formation/oxidation of oxygenated fuels in a cylindrical constant volume chamber. *Fuel 167* (2016), 49 – 59.

[23] Jacobs, S., and Heufer, K. A. *Combust. Flame* (2017).

[24] Jr., D. M. M., and Kilpatrick, J. E. Entropy and related thermodynamic properties of dimethoxymethane. *J. Chem. Phys. 41*, 10 (1964), 3127–3131.

[25] Kopp, W. A., Langer, R. T., Döntgen, M., and Leonhard, K. Hydrogen abstraction from n-butyl formate by $h^{\cdot}$ and $ho_2^{\cdot}$. *J. Phys. Chem. A 117* (2013), 6757–6770.

[26] Lacher, J. R. The chemical thermodynamics of organic compounds (stull, daniel r.; westrum, edgar f.;

sinke, gerard c.). *J. Chem. Educ. 47*, 4 (1970), A300.

[27] Lee, T. J., and Taylor, P. R. A diagnostic for determining the quality of single-reference electron correlations methods. *Int. J. Quantum Chem. 23* (1989), 199–207.

[28] Li, Q. S., Zhang, Y., and Zhang, S. Dual level direct *ab initio* and density-functional theory dynamics on the unimolecular decomposition of CH_3OCH_2 radical. *J. Phys. Chem. A 108* (2004), 2014–2019.

[29] Liu, H., Wang, Z., Wang, J., and He, X. Improvement of emission characteristics and thermal efficiency in diesel engines by fueling gasoline/diesel/PODEn blends. *Energy 97* (FEB 15 2016), 105–112.

[30] Lumpp, B., Rothe, D., Pastötter, C., Lämmermann, R., and Jacob, E. Oxymethylenether als dieselkraftstoffzusätze der zukunft. *MTZ Motortech. Z 72* (2011), 198.

[31] Marrodán, L., Monge, F., Millera, A., Bilbao, R., and Alzueta, M. U. Dimethoxymethane Oxidation in a Flow Reactor. *Combust. Sci. Technol. 188*, 4-5, SI (2016), 719–729. 9th Mediterranean Combustion Symposium, Rhodes, GREECE, JUN 07-11, 2015.

[32] Marrodán, L., Royo, E., Millera, A., Bilbao, R., and Alzueta, M. U. High Pressure Oxidation of Dimethoxymethane. *Energ. Fuel 29*, 5 (MAY 2015), 3507–3517.

[33] Miller, J. A., and Klippenstein, S. J. Determining phenomenological rate coefficients from a time-dependent, multiple-well master equation: "species reduction" at high temperatures. *Phys. Chem. Chem. Phys. 15* (2013), 4744–4753.

[34] Neese, F., Schwabe, T., and Grimme, S. Analytic derivatives for perturbatively corrected double hybrid density functionals: Theory, implementation, and applications. *J. Chem. Phys. 126*, 12 (2007), 124115.

[35] Peukert, S. L., Sivaramakrishnan, R., Su, M.-C., and Michael, J. V. Experiment and theory on methyl-formate and methylacetate kinetics at high temperatures: Rate constants for h-atom abstraction and thermal decomposition. *Combust. Flame 159*, 7 (2012), 2312 – 2323.

[36] Pfahl, U., Fieweger, K., and Adomeit, G. Self-ignition of diesel-relevant hydrocarbon-air mixtures under engine conditions. *Symposium (International) on Combustion 26*, 1 (1996), 781 – 789.

[37] Pilcher, G., and Fletcher, R. A. Measurements of heats of combustion by flame calorimetry. part 5.-dimethoxymethane, 1,1-dimethoxyethane. *Trans. Faraday Soc. 65* (1969), 2326–2330.

[38] Ren, Y., Huang, Z., Miao, H., Di, Y., Jiang, D., Zeng, K., Liu, B., and Wang, X. Combustion and emissions of a {DI} diesel engine fuelled with diesel-oxygenate blends. *Fuel 87*, 12 (2008), 2691 – 2697.

[39] Schmitz, N., Burger, J., and Hasse, H. Reaction kinetics of the formation of poly(oxymethylene) dimethyl ethers from formaldehyde and methanol in aqueous solutions. *Ind. Eng. Chem. Res. 54*, ‘ (2015), 12553–12560.

[40] Schmitz, N., Homberg, F., Berje, J., Burger, J., and Hasse, H. Chemical equilibrium of the synthesis of poly(oxymethylene) dimethyl ethers from formaldehyde and methanol in aqueous solutions. *Ind. Eng. Chem. Res. 54* (2015), 6409–6417.

[41] Seal, P., Papajak, E., and Truhlar, D. G. Kinetics of the hydrogen abstraction from carbon-3 of 1-butanol by hydroperoxyl radical: Multi-structural variational transition-state calculations of a reaction with 262 conformations of the transition state. *J. Phys. Chem. Lett. 3* (2012), 264–271.

[42] Thomas, P. S., and Carrington, T. Using nested contractions and a hierarchical tensor format to compute vibrational spectra of molecules with seven atoms. *J. Phys. Chem. A 119*, 52 (2015), 13074–13091. PMID: 26555177.

[43] Umer, M., Kopp, W. A., and Leonhard, K. Efficient yet accurate approximations for ab initio calculations of alcohol cluster thermochemistry. *J. Chem. Phys. 143* (2015), 214306.

[44] Van Speybroeck, V., Vansteenkiste, P., Van Neck, D., and Waroquier, M. Why does the uncoupled hindered rotor model work well for the thermodynamics of *n*-alkanes? *Chem. Phys. Lett. 402* (2005), 479–484.

[45] Vandeputte, A. G., Sabbe, M. K., Reyniers, M.-F., Van Speybroeck, V., Waroquier, M., and Marin, G. B. Theoretical study of the thermodynamics and kinetics of hydrogen abstractions from hydrocarbons. *J. Phys. Chem. A 111* (2007), 11771–11786.

[46] Vansteenkiste, P., Van Speybroeck, V., Marin, G. B., and Waroquier, M. Ab initio calculation of entropy and heat capacity of gas-phase *n*-alkanes using internal rotations. *J. Phys. Chem. A 107* (2003), 3139–3145.

[47] Wang, H. W., Zhou, L. B., Jiang, D. M., and Huang, Z. H. Study on the performance and emissions of a compression ignition engine fuelled with dimethyl ether. *Proceedings of the Institution of Mechanical Engineers, Part D: Journal of Automobile Engineering 214*, 1 (2000), 101–106.

[48] Yamada, T., Bozzelli, J., and Lay, T. Comparisons of CBS-q and G2 calculations on thermodynamic properties, transition states, and kinetics of dimethyl-ether plus O-2 reaction system. *Int. J. Chem. Kinet. 32*, 7 (JUL 2000), 435–452.

[49] Yan, J., Lee, D., Chou, S., Desideri, U., Li, H., Zhang, X., Kumar, A., Arnold, U., and Sauer, J. International conference on applied energy, icae2014 biomass-derived oxymethylene ethers as diesel additives: A thermodynamic analysis. *Energy Procedia 61* (2014), 1921 – 1924.

[50] Yan, J., Shamim, T., Chou, S., Li, H., Wang, Z., Liu, H., Zhang, J., Wang, J., and Shuai, S. Clean, efficient and affordable energy for a sustainable future: The 7th international conference on applied energy (icae2015) performance, combustion and emission characteristics of a diesel engine fueled with polyoxymethylene dimethyl ethers (pode3-4)/ diesel blends. *Energy Procedia 75* (2015), 2337 – 2344.

[51] Yasunaga, K., Simmie, J. M., Curran, H. J., Koike, T., Takahashi, O., Kuraguchi, Y., and Hidaka, Y. Detailed chemical kinetic mechanisms of ethyl methyl, methyl *tert*-butyl and ehtyl *tert*-butyl ethers: The importance of uni-molecular elimination reactions. *Combust. Flame 158* (2011), 1032–1036.

[52] Zhao, Y., and Truhlar, D. G. The m06 suite of density functionals for main group thermochemistry,

thermochemical kinetics, noncovalent interactions, excited states, and transition elements: two new functionals and systematic testing of four m06-class functionals and 12 other functionals. *Theor. Chem. Acc. 120*, 1 (2008), 215–241.

[53] Zheng, J., Zhao, Y., and Truhlar, D. G. The dbh24/08 database and its use to assess electronic structure model chemistries for chemical reaction barrier heights. *J. Chem. Theory Comput. 5*, 4 (2009), 808–821.